



# Daytime HONO, NO<sub>2</sub> and aerosol distributions from MAX-DOAS observations in Melbourne

Robert G. Ryan<sup>1,2</sup>, Steve Rhodes<sup>3</sup>, Matthew Tully<sup>3</sup>, Stephen Wilson<sup>4</sup>, Nicholas Jones<sup>4</sup>, Udo Frieß<sup>5</sup>, and Robyn Schofield<sup>1,2</sup>

<sup>1</sup>School of Earth Sciences, University of Melbourne, Melbourne, Australia

<sup>2</sup>ARC Centre of Excellence for Climate System Science, Sydney, Australia

<sup>3</sup>Bureau of Meteorology, Melbourne, Australia

<sup>4</sup>School of Chemistry, University of Wollongong, Wollongong, Australia

<sup>5</sup>Institute for Environmental Physics, University of Heidelberg, Heidelberg, Germany

**Correspondence:** Robert G. Ryan (rgryan@student.unimelb.edu.au)

Received: 24 April 2018 – Discussion started: 18 May 2018

Revised: 9 August 2018 – Accepted: 11 September 2018 – Published: 2 October 2018

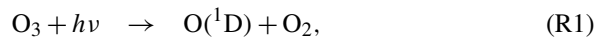
**Abstract.** Toxic nitrogen oxides produced by high temperature combustion are prevalent in urban environments, contributing to a significant health burden. Nitrogen oxides such as NO<sub>2</sub> and HONO in pollution are important for hydroxyl radical (OH) production and overall oxidative capacity in urban environments; however, current mechanisms cannot explain high daytime levels of HONO observed in many urban and rural locations around the world. Here we present HONO, NO<sub>2</sub> and aerosol extinction vertical distributions retrieved from multi-axis differential optical absorption spectroscopy (MAX-DOAS) measurements in suburban Melbourne, which are the first MAX-DOAS results from the Australian continent. Using the optimal estimation algorithm HEIPRO we show that vertical profiles for NO<sub>2</sub> and HONO can be calculated with a low dependence on the retrieval forward model and a priori parameters, despite a lack of independent co-located aerosol or trace gas measurements. Between December 2016 and April 2017 average peak NO<sub>2</sub> values of  $8 \pm 2$  ppb indicated moderate traffic pollution levels, and high daytime peak values of HONO were frequently detected, averaging  $220 \pm 30$  ppt in the middle of the day. HONO levels measured in Melbourne were typically lower than those recorded in the morning in other places around the world, indicating minimal overnight accumulation, but peaked in the middle of the day to be commensurate with midday concentrations in locations with much higher NO<sub>2</sub> pollution. Regular midday peaks in the diurnal cycle of HONO surface concentrations have only previously been

reported in rural locations. The HONO measured implies a daytime source term  $1 \text{ ppb h}^{-1}$  above the predicted photo-stationary state (PSS) concentration and represents an OH radical source up to 4 times stronger than from ozone photolysis alone in the lowest 500 m of the troposphere. The dependence of the high midday HONO levels on soil moisture, combined with the observed diurnal and vertical profiles, provides evidence for a strong photoactivated and ground-based daytime HONO source.

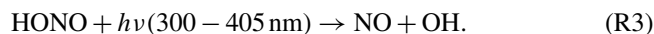
## 1 Introduction

The World Health Organization indicates that ambient air pollution exposure represents the largest environmental risk to human health, with as many as one in nine deaths attributable to poor air quality (WHO, 2016). In Australia, with isolated but highly urbanised population centres, the economic cost of mortality attributed to air pollution is estimated to be of the order of Dollars AUD 11–24 billion per year (Begg et al., 2007; AccessEconomics, 2008). This makes understanding the oxidation chemistry underpinning urban pollution processes, and particularly closing the budget of chemical oxidants in urban areas, a priority for atmospheric scientists. The oxidative capacity of the atmosphere is primarily determined by the hydroxyl radical (OH). However, the sources and sinks of OH in many environments remain uncertain. Ozone photolysis, through Reactions (R1) and (R2),

is often considered to be the primary pathway for OH formation in the atmospheric boundary layer:



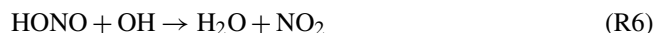
Several studies have identified higher daytime nitrous acid (HONO) levels in urban areas than can be explained by the known mechanisms, indicating an unknown daytime HONO source (Lee et al., 2016; Acker and Möller, 2007; Kleffmann, 2007; Wong et al., 2012; Huang et al., 2017; Neuman et al., 2016). Given that HONO photolysis (Reaction R3) is a strong OH source, elevated daytime HONO levels can significantly increase the local tropospheric oxidative capacity:



Major known HONO sources include direct emission from combustion engines, the daytime homogeneous Reaction (R4) and the heterogeneous Reaction (R5) occurring where water is adsorbed to surfaces (H<sub>2</sub>O<sub>(ads)</sub>).



HONO sinks include dry deposition, photolysis to produce OH (Reaction R3) and reaction with OH (Reaction R6).



Since Reaction (R6) is very slow (rate =  $k[\text{OH}] \approx 10^{-16} \text{ s}^{-1}$ , where  $k$  is the rate constant) compared to Reaction (R3) (photolysis rate  $J(\text{HONO}) \approx 3 \times 10^{-5} \text{ s}^{-1}$  around midday) (Sander et al., 2006), photolysis is the dominant daytime sink process. Consequently, HONO accumulating overnight rapidly photolyses in the early morning, and HONO concentrations are expected to decrease with increasing UV radiation. While observed daytime HONO decreases from an early morning maximum, many studies have still observed higher-than-expected daytime HONO concentrations, with a missing source component peaking around the middle of the day (e.g. Li et al., 2012; Qin et al., 2009; Lee et al., 2016; Hendrick et al., 2014; Pinto et al., 2014). Maximum diurnal HONO mixing ratios have been reported during the late morning and middle of the day in Cyprus (Meusel et al., 2016) and at a rural site in Germany (Acker et al., 2006). Studies have suggested that the missing source may be related to heterogeneous chemistry involving water, aerosols, ground surfaces (e.g. Reaction R5) or soil-based emissions. To assess the feasibility of these potential HONO sources, reliable vertical gradient measurements of HONO and its precursors, including nitrogen dioxide (NO<sub>2</sub>), are required. To address this need, in recent times, passive monitoring techniques such as multi-axis differential optical absorption spectroscopy (MAX-DOAS) have risen to prominence.

The MAX-DOAS technique relies on measurements of scattered sunlight in the ultraviolet and visible wavelengths (UV-vis), at several viewing angles, facilitating the retrieval of vertical information on tropospheric aerosol extinction and trace gas concentration (Platt and Stutz, 2008; Hönninger et al., 2004). Variations in light pathlength due to aerosol scattering are inferred from absorption measurements of the O<sub>2</sub> collision complex O<sub>4</sub>, whose concentration has a well-defined relationship with atmospheric pressure (Wagner et al., 2004; Frieß et al., 2006). The retrieved aerosol information can then be used as input to estimate vertical concentration profiles for UV-vis-absorbing trace gases including NO<sub>2</sub>, HONO, formaldehyde, glyoxal and bromine monoxide (e.g. Vlemmix et al., 2015; Hendrick et al., 2014; Schreier et al., 2016; Jin et al., 2016).

NO<sub>2</sub> has been well studied using MAX-DOAS in many locations around the world due to its strong UV absorbance and its ubiquity as an urban pollutant (e.g. Ma et al., 2013; Vlemmix et al., 2015; Kanaya et al., 2014; Wagner et al., 2011; Ortega et al., 2015). In contrast, nitrous acid has more commonly been studied using active, long-path DOAS due to its lower concentration and weaker absorbance (Platt and Perner, 1983; Kleffmann et al., 2006; Stutz et al., 2010). Recently, attention has turned to studying nitrous acid using MAX-DOAS, in a HONO slant column intercomparison during the MAD-CAT (Multi-Axis DOAS – Comparison campaign for Aerosols and Trace gases) campaign held in 2013 in Mainz, Germany (Wang et al., 2017), and in HONO and NO<sub>2</sub> profile retrievals in Beijing, China (Hendrick et al., 2014), and Madrid, Spain (Garcia-Nieto et al., 2018). The findings of Hendrick et al. (2014) were in line with previous published HONO data from long-path DOAS and in situ measurements, showing higher-than-expected HONO concentrations and indicating an unaccounted source of daytime HONO (e.g. Lee et al., 2016; Acker and Möller, 2007; Kleffmann, 2007; Wong et al., 2012; Huang et al., 2017; Neuman et al., 2016). Considerable efforts have been made to determine the mechanism of the missing source(s) and the importance of HONO as a tropospheric radical source through vertical gradient measurements using long-path DOAS (Stutz et al., 2010; Wong et al., 2012; Young et al., 2012), aeroplanes (Neuman et al., 2016), Zeppelins (Li et al., 2014) and towers (Kleffmann et al., 2003; VandenBoer et al., 2013).

Compared to these expensive, short-term campaign platforms, MAX-DOAS measurements of HONO vertical profiles as demonstrated in Hendrick et al. (2014) and Garcia-Nieto et al. (2018) have the significant advantages of simple autonomous instrumentation, being cheap to run and able to be deployed in any environment for long-term monitoring programmes. However, the MAX-DOAS method has some drawbacks which include complicated, multistep data processing, limited information content from which to derive vertical profile information and interference from clouds. The choice of a priori and forward model parameters can also introduce retrieval errors especially in the absence of exter-

nal co-located aerosol and trace gas measurements (Ortega et al., 2016; Wagner et al., 2011).

While MAX-DOAS has been deployed across much of the Northern Hemisphere, there are few reports of DOAS and HONO observations from the Southern Hemisphere. In this paper measurements are presented from Melbourne, which are, to the best of our knowledge, the first MAX-DOAS results published from the Australian continent. Melbourne, the capital of Victoria, is the second largest city in Australia with over 4.8 million people, accounting for 19 % of the national population. The Victorian Environmental Protection Agency (EPA) has been monitoring air quality, including nitrogen oxide levels at several different sites around the Melbourne metropolitan area since 1979 (see map in Fig. 1). In that time, average annual NO<sub>2</sub> levels have decreased from 13 ppb to below 10 ppb, despite significant population and vehicle number increases (EPA, 2013), which is attributed to improved vehicle pollution reduction technology and fuel efficiency. With the Australian National Environment Protection Measure Standards annual average NO<sub>2</sub> concentration at 30 ppb, these figures indicate that Melbourne has good air quality as far as nitrogen oxides are concerned. On the one hand, this provides an ideal opportunity to study the oxidation budget of HONO and OH in a low to moderately polluted urban environment. On the other hand, addressing the paucity of air quality data in Melbourne is important given that epidemiological studies have demonstrated correlations between particulates and NO<sub>2</sub> pollution on overall mortality (Simpson et al., 2000, 2005) and cardiovascular disease (e.g. Barnett et al., 2006) in Melbourne. The results presented in this paper demonstrate the ability of MAX-DOAS measurements to provide important air quality data in Melbourne and contribute to an improved understanding of how HONO impacts the budget of tropospheric oxidants.

## 2 Measurement and profile retrieval details

### 2.1 Measurement site and MAX-DOAS instrumentation

The Australian Bureau of Meteorology (BOM) has operated a MAX-DOAS instrument in Broadmeadows, a northern suburb of Melbourne, since August 2016. Results are presented in this work from December 2016 to April 2017. The instrument is mounted on a laboratory roof looking in a south-westerly direction over one of Melbourne's main arterial motorways (the Western Ring Road) and, further to the south, the northern suburbs and central city as shown in Fig. 1. Located close to the Western Ring Road, the MAX-DOAS is ideally placed to measure the resulting traffic pollution plumes. Being on the northern fringes of the Melbourne metropolitan area, the instrument is well situated to study the interaction of rural and urban air masses given prevailing northerly or southerly winds respectively.



**Figure 1.** (a) Map of Australia showing the location of Melbourne. (b) Map of the Melbourne metropolitan area showing the location of the Broadmeadows measurement site (yellow marker) in the northern suburbs. The red arrow shows the south–south-west viewing direction of the MAX-DOAS instrument. The blue markers indicate the four Victorian EPA NO<sub>2</sub> measurement sites, which are referred to in the results section.

The MAX-DOAS used in this work was a commercial 1-D instrument manufactured by the German company Environmental Measurement Systems (Envimes). The instrument consists of a scanner telescope box, looking towards a fixed compass direction of 208 degrees, connected by fibre optic and data cables to spectrometer and computer units inside the laboratory. The spectrometer unit contained temperature-stabilised 75 mm Avantes spectrometers for UV (295–450 nm, 0.6 nm resolution) and visible (430–565 nm, 0.6 nm resolution) regions. The UV detector was a Hamamatsu back-thinned detector with a Schott BG3 filter and 2048 pixel channels while the visible detector was a Sony 2048L also with 2048 channels. The telescope unit contains a rotating prism and inclinometer facilitating active elevation control with quoted elevation angle accuracy < 0.1°. Similar commercial-grade Envimes MAX-DOAS instruments have demonstrated good performance at the MAD-CAT intercomparison campaign in Mainz, Germany (Lampel et al., 2015; Wang et al., 2017). Wavelength calibrations were carried out using an external mercury lamp, and spectra were corrected for detector non-linearity, dark current and spectral offset using laboratory measurements. The measurement sequence was controlled using the MS-DOAS software custom designed by Envimes, and it consisted of a set of elevation angle scans at 90, 30, 20, 10, 5, 3 and 2° which took approximately 12 min to complete.

### 2.2 DOAS fitting

The DOAS technique allows the Beer–Lambert law to be applied in an atmospheric context, with low-frequency attenuation components of the scattered light spectra (such as Rayleigh and Mie scattering) being separated from the high-frequency trace gas absorptions (Platt and Stutz, 2008). The low-frequency component is approximated using a poly-

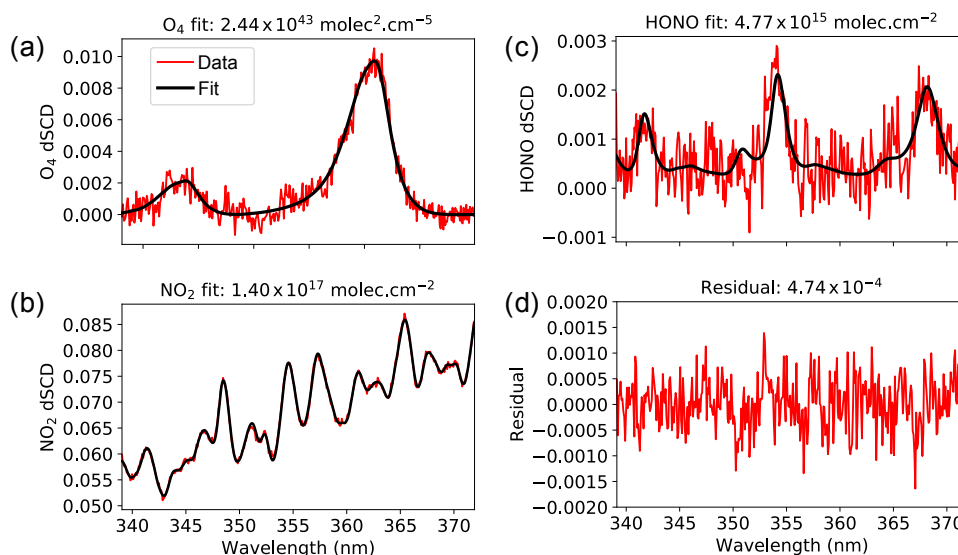


**Figure 2.** Example DOAS fit results for a 2° elevation angle and 28° solar zenith angle on 4 March 2017, showing (a) O<sub>4</sub> and (b) NO<sub>2</sub> in the 338–370 nm fitting window, with (c) HONO and (d) fit residual in the 339–372 nm fitting range.

nomial, while the high-frequency component is fitted with the relevant trace gas absorption cross sections using a least squares fitting algorithm (see Fig. S1a in the Supplement). The resulting value is the differential slant column density (dSCD), which is the light-path integrated trace gas concentration, relative to a reference spectrum. In the case of MAX-DOAS measurements the reference spectrum is typically the 90° spectrum in each scan set, effectively cancelling out the stratospheric influence and allowing the retrieval of tropospheric specific information (Platt and Stutz, 2008).

DOAS analysis was carried out using the QDOAS software developed at the Royal Belgian Institute for Space Aeronomy (BIRA-IASB; version 2.111, April 2016, <http://uv-vis.aeronomie.be/software/QDOAS/>), using cross sections convolved with the instrumental slit function (cross sections are listed in Table S1 in the Supplement). The UV wavelength range 338–370 nm was used in the analysis for NO<sub>2</sub> and O<sub>4</sub>, based on recommended settings from the CINDI intercomparison campaign (Roscoe et al., 2010), with the inclusion of the HONO cross section and a temperature-dependent ring term as in Volkamer et al. (2015) and Lampel et al. (2017). A sensitivity study to optimise the HONO fitting wavelength range was performed using the retrieval interval mapping technique of Vogel et al. (2013) (Supplement Fig. S1b), which showed that the smallest HONO fit percentage errors correspond to a wavelength range starting below 340 nm. An inspection of the fitted cross sections (see Fig. S1c in the Supplement) shows that the HONO fit error is improved by including all three of the largest HONO cross-section peaks, despite the 341 nm HONO peak overlapping with formaldehyde and O<sub>4</sub> features. This is in line with Wang et al. (2017) and Hendrick et al. (2014), although the fitting

window 339–372 nm chosen here for HONO is shorter than in these papers in order to minimise the overall residual root mean squared (rms) error of the fits, while maintaining low HONO fit errors.

Successful DOAS retrievals for O<sub>4</sub>, NO<sub>2</sub> and HONO are demonstrated in Fig. 2. In the 339–372 nm fitting window, over the measurement period HONO retrieval errors for solar zenith angles (SZAs) < 80° averaged between 17 % and 25 %, from elevation angles 2 to 30°. These results are not filtered for the influence of clouds. The fits shown in Fig. 2 and separation between dSCDs of different elevation angles shown in Fig. 3 indicate the successful retrieval of HONO slant columns. NO<sub>2</sub> and O<sub>4</sub> fitting errors were typically of the order of 2 % throughout the measurement period, and residual rms values averaged  $(5.4 \pm 1.1) \times 10^{-4}$  but were typically  $< 4.8 \times 10^{-4}$  in the middle of the day as in Fig. 2d, for all elevation angles.

### 2.3 Profile retrieval

A commonly used strategy to retrieve vertical information from MAX-DOAS measurements involves using a radiative transfer model (RTM) as a forward model **F** to simulate trace gas slant columns. The simulated and measured slant columns are then inverted to calculate a vertical trace gas profile, for example using the optimal estimation method (Rodgers, 1990, 2000; Frieß et al., 2006; Wagner et al., 2004). In order to retrieve trace gas vertical profiles in this way, information on the atmospheric aerosol extinction is needed to constrain the light path. The solution for the aerosol profile **x** is calculated iteratively by varying the aerosol input parameters until best agreement is found between the measurement vector **y** and the RTM simulations.

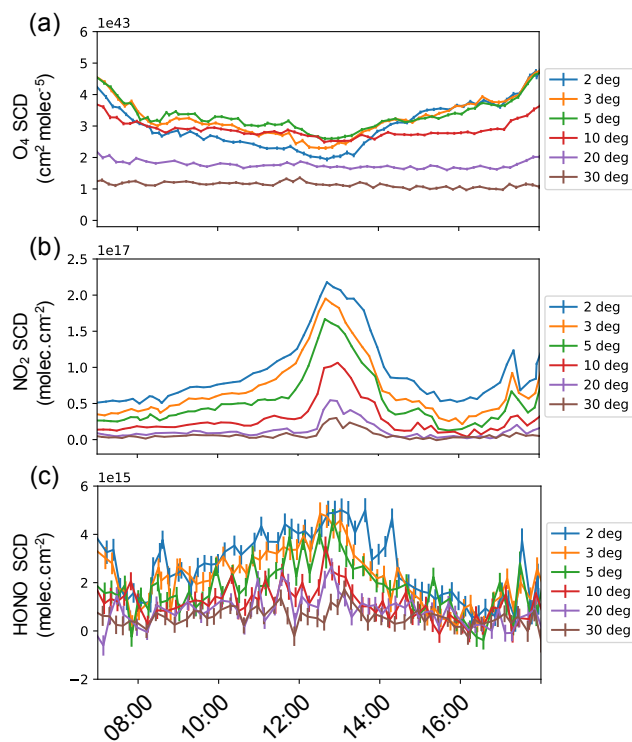


**Figure 3.** Diurnal differential slant column profiles for (a) O<sub>4</sub>, (b) NO<sub>2</sub> and (c) HONO for 4 March 2017.

The agreement is quantified by minimising the cost function  $\chi^2$ :

$$\chi^2 = (\mathbf{y} - \mathbf{F}(\mathbf{x}))^T \mathbf{S}_\epsilon^{-1} (\mathbf{y} - \mathbf{F}(\mathbf{x})) + (\mathbf{x} - \mathbf{x}_a)^T \mathbf{S}_a^{-1} (\mathbf{x} - \mathbf{x}_a). \quad (1)$$

In Eq. (1),  $\mathbf{x}_a$  is a priori information which must be provided to constrain the inversion algorithm because the problem is ill-posed.  $\mathbf{S}_a$  and  $\mathbf{S}_\epsilon$  represent the error covariance matrices of the a priori and measurement vectors respectively. The averaging kernel matrix  $\mathbf{A} = \frac{\partial \hat{\mathbf{x}}}{\partial \mathbf{x}}$  represents the sensitivity of the retrieved profile  $\hat{\mathbf{x}}$  to the true profile  $\mathbf{x}$  such that

$$\hat{\mathbf{x}} = \mathbf{x}_a + \mathbf{A}(\mathbf{x} - \mathbf{x}_a). \quad (2)$$

The information content of a retrieval can be quantified by the degrees of freedom for signal (DoF), which is the trace of  $\mathbf{A}$ . The profile retrievals in this work were carried out using the HEIPRO algorithm, as described in Frieß et al. (2006), which uses the radiative transfer code SCIATRAN (Rožanov et al., 2014) as the forward model. To ensure agreement between modelled and measured O<sub>4</sub> dSCDs, simulations in HEIPRO with different cross-sectional scaling factors were carried out as in Wang et al. (2016). It was found that a cross-sectional scaling factor of 0.80 on the Hermans et al. (2003) O<sub>4</sub> cross section used to model dSCDs in SCIATRAN consistently brought the measured O<sub>4</sub> dSCDs, fitted using the Thalman and Volkamer (2013) O<sub>4</sub> cross section, into agreement.

Aerosol retrievals from O<sub>4</sub> were calculated at 360.8 nm, NO<sub>2</sub> retrievals at 365.4 nm and HONO retrievals at 354.3 nm. HEIPRO was configured to retrieve profiles over 20 layers from 0.1 to 3.9 km, using elevation angle sets of 90, 30, 20, 10, 5, 3 and 2°. For all retrievals, a fixed exponentially decreasing a priori profile, characterised by a ground concentration (or ground extinction in the case of aerosols), and a scale height were used to initialise the retrieval. A scale height of 0.6 km was chosen for all retrievals, and the surface parameter (i.e. surface extinction for aerosols, surface concentration for trace gases) varied for each retrieved species. The impact of the choice of these a priori and other forward model parameters is discussed in further detail in the results section. Construction of the measurement error covariance matrix  $\mathbf{S}_\epsilon$  assumed that measurement errors were independent of each other, with diagonal elements equal to the square of the DOAS fit error. The a priori error covariance matrix  $\mathbf{S}_a$  was constructed as described by Frieß et al. (2006) with the variance set to 100 % for all altitudes in order to allow for deviations from the a priori profile in the case of high aerosol optical depths (AODs), while minimising opportunities for the algorithm to fit noise.

### 3 Results and discussion

#### 3.1 Vertical distribution of aerosols, NO<sub>2</sub> and HONO

A 3-month dataset of MAX-DOAS measurements from Broadmeadows was analysed for aerosols, HONO and NO<sub>2</sub>. Results were screened for the likely presence of cloud by applying a filter based on the colour index (CI), defined as the ratio between spectral intensities at 330 and 390 nm (Wagner et al., 2016). Diurnal CI thresholds were determined for each of the 3 months in the campaign period by fitting a fifth-order threshold polynomial to CI data from clear days as a function of time. Data were filtered out where the CI was less than 10 % of the threshold CI polynomial at the given time. Despite the lack of co-located external solar radiation data, cloud-flagged periods determined using the MAX-DOAS-measured CI filter corresponded with low global radiation measured at Melbourne Airport, 6 km west of Broadmeadows, giving confidence in the simple empirical cloud filtering approach used here.

The considerable advantage of MAX-DOAS over other methods of measuring HONO is the ability to simultaneously and passively measure vertical distributions of HONO, NO<sub>2</sub> and aerosols. Figure 4 shows some example retrieval results from HEIPRO, for 7 March, a clear day. The profile retrievals are dominated by the layers closest to the ground, as expected given that the averaging kernels show greatest sensitivity in the lowest  $\approx 1$  km for aerosol extinction and NO<sub>2</sub> and the lowest  $\approx 500$  m for HONO. The high DoF found for the aerosol and NO<sub>2</sub> retrieval gives confidence in the retrieval result. While the DoF for HONO is lower than for NO<sub>2</sub>, this

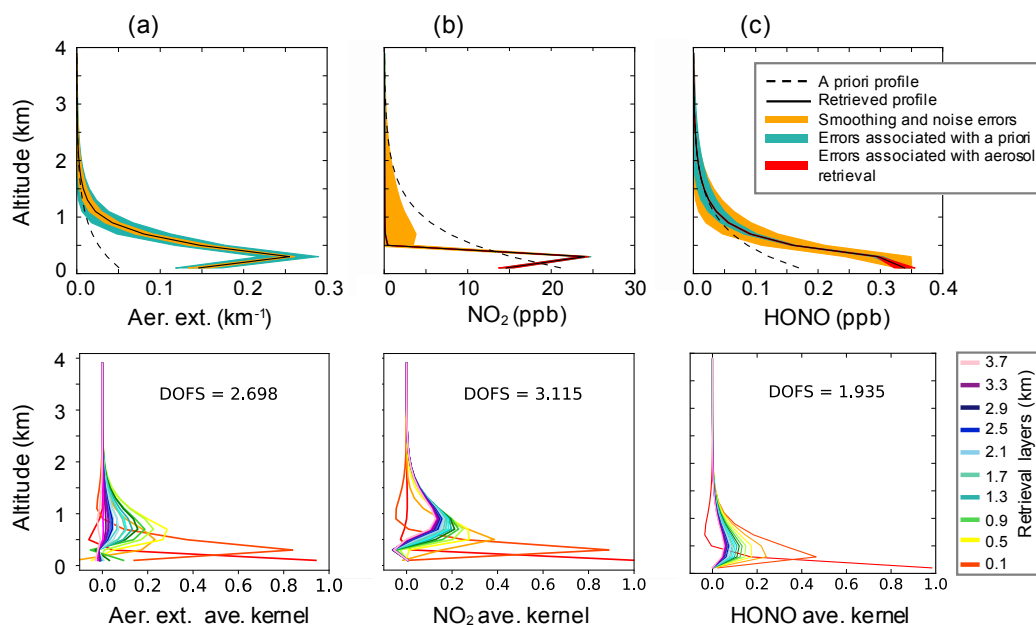


**Figure 4.** Example profile retrieval results from 13:00 LT on 7 March 2017 at Broadmeadows, for (a) aerosol extinction (aer. ext.), (b) NO<sub>2</sub> and (c) HONO. The top row shows the retrieved profiles, plotted with their associated a priori profile, smoothing and noise errors, and the errors associated with uncertainty in the a priori profile as calculated during the retrieval sensitivity tests. The trace gas profiles also include the error associated with total uncertainty in aerosol forward model parameters and uncertainty in the aerosol retrieval. The bottom row presents the averaging kernels and degrees of freedom for signal associated with the profile retrieval. The averaging kernels' legend represents the centre wavelength of every second retrieval grid layer, for clarity.

result is comparable to the DoF found for the MAX-DOAS HONO retrieval in Beijing by Hendrick et al. (2014), wherein the difference is attributed to the much greater absorption strength of NO<sub>2</sub> compared to HONO.

With no appropriate co-located measurements, the choice of a priori and forward model parameters is a source of uncertainty propagating through both the aerosol and trace gas profile retrievals (Ortega et al., 2016; Wagner et al., 2011). In this work, a sensitivity study was undertaken to examine the relative contribution of different a priori and forward model parameters on the final aerosol and trace gas retrieval products using the optimal estimation method. The parameters investigated were the surface albedo, aerosol optical properties, aerosol profile shape and trace gas profile shape. The tests involved running aerosol and trace gas retrievals in HEIPRO over 3 sunny days of measurements at Broadmeadows, varying each parameter separately. Preliminary HEIPRO retrievals for March 2017 were used to determine ranges for the a priori shape parameters, including a scale height ranging from 0.4 to 0.8 km and ground extinction ranging from 0.04 to 0.08 km<sup>-1</sup>. Ranges for the aerosol optical property tests were determined from AERONET data taken between 2003 and 2017 at six different sites around south-eastern Australia, giving an asymmetry parameter of 0.66–0.75 and a single scattering albedo of 0.7–1.0, consistent with the ranges discussed for different aerosol types over

the Australian continent in Qin and Mitchell (2009). Surface albedo range limits of 0.05 and 0.2 were chosen, consistent with field observations of urban surface albedo over grass and motorways respectively (Feister and Grewe, 1995).

For the aerosol profile retrieval, uncertainty in the aerosol a priori shape parameters was found to contribute the most significant error at high altitudes, where the information content provided to the retrieval algorithm by the measurements is lowest (see full sensitivity test results in the Supplement). In the lowest 500 m, the combined error due to uncertainty in a priori aerosol shape and forward model parameters was found to be 17 %, as shown alongside the 6 % smoothing and noise error in Fig. 4. The combined smoothing and noise errors shown in Fig. 4 add up to 10 % of the retrieved profile in the lowest 500 m for NO<sub>2</sub>, and 15 % for HONO, in good agreement with the values found in Hendrick et al. (2014). It is pleasing to note that the influence of the propagating aerosol error and trace gas shape a priori parameters is between 3 % and 4 % for each case and for both trace gases. This suggests that the HONO and NO<sub>2</sub> low-altitude concentrations are largely independent of the aerosol and trace gas input parameters, giving confidence in the HEIPRO retrieval approach.

The example vertical profiles presented in Fig. 4 are typical for sunny days during the measurement period where aerosol extinction and NO<sub>2</sub> were often found to peak above

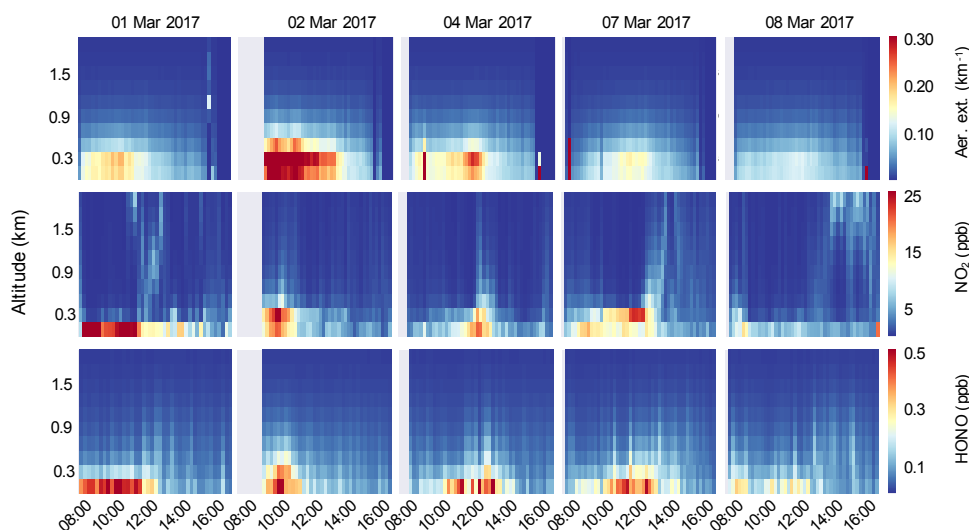


**Figure 5.** Example vertical profile time series, plotted as heat maps with altitude on the y axis, for selected mostly sunny days in early March 2017. The top row shows aerosol extinction, the middle row the NO<sub>2</sub> mixing ratio and the bottom row the HONO mixing ratio.

ground level and HONO was found to peak at ground level. The elevated location of the measurement site overlooking the city to the south makes these profile shapes plausible, suggesting that the instrument is sampling the particulate and NO<sub>2</sub> pollution plume of Melbourne. The typical HONO profile shape peaking at ground level could be a function of the greater retrieval sensitivity bias for HONO compared to NO<sub>2</sub> and aerosols. It could also indicate that HONO sources are ground based, with strong HONO photolysis not allowing the same daytime vertical gradients as NO<sub>2</sub> and aerosols.

As expected given the profile retrieval sensitivity discussed above, almost all the retrieved aerosol extinction, HONO and NO<sub>2</sub> are in the lower troposphere, as shown in example vertical profile heat maps in Fig. 5. The diurnal variation of the aerosol profiles shown on these example days in early March 2017 is typical of the profiles throughout the measurement period. Aerosol extinction commonly peaked temporally in the late morning, and vertically at about 300 m, suggesting that from the elevated measurement position at Broadmeadows the MAX-DOAS is sampling an evolving boundary layer and aerosol pollution plume over the city of Melbourne. NO<sub>2</sub> peaks often correspond well, both temporally and vertically, with aerosol extinction. HONO retrievals are most sensitive to the lowest layer and consequently retrieved HONO peaks are always at the ground level. The strong HONO vertical gradient is also consistent with previous measurements made using various techniques and platforms (e.g. Wong et al., 2012; Hendrick et al., 2014; Garcia-Nieto et al., 2018; Stutz et al., 2010; Young et al., 2012; Neuman et al., 2016; Li et al., 2014; Kleffmann et al., 2003; VandenBoer et al., 2013). Elevated NO<sub>2</sub> and aerosol layers could indicate that they are more likely to be influenced by longer range transport than HONO. Mixing layer heights were es-

timated as  $H_{ML} \approx c \times (VCD/x(\text{ppb}))$ , following the method of Li et al. (2013), where  $x(\text{ppb})$  is the trace gas mixing ratio in the lowest retrieval layer and  $c$  is the conversion factor between molecules  $\text{cm}^{-3}$  and ppb. Regression analysis using the Deming method showed that  $H_{ML}$  values for HONO and NO<sub>2</sub> were weakly correlated (Pearson's  $R$  coefficient 0.42), with a slope of 1.65 indicating that  $H_{ML}$  was typically higher for NO<sub>2</sub> than HONO. This is consistent with the correlation of vertical column density to surface mixing ratio, which is 0.89 for HONO and 0.79 for NO<sub>2</sub>, suggesting that surface values are a greater influence on the total column for HONO than NO<sub>2</sub>. This is also consistent with previous findings that HONO production is dominated by surface rather than upper level processes such as aerosol-mediated conversion of NO<sub>2</sub> (e.g. Michoud et al., 2014; Lee et al., 2016).

### 3.2 Comparison with external data

In the case of Melbourne few options exist for the validation of the MAX-DOAS data. For aerosol optical depth the MAX-DOAS results were compared with retrieval products from the MODIS (Moderate Resolution Imaging Spectroradiometer) Terra satellite at the time of satellite overpass ( $\approx 14:00$  LT daily). For a measurement period as short as 3 months, such comparisons are of limited usefulness since satellite overpasses occur only once a day, and the wavelength of the MODIS corrected optical depth over land was 440 nm while the MAX-DOAS AOD retrieval was at 360 nm in this study. Regression analysis was conducted using the Deming method which, unlike the simple linear least squares regression, assumes a measurement error in both  $x$  and  $y$  variables. It also allows for the regression to be weighted by the ratio of variances (RV) between the independent and de-

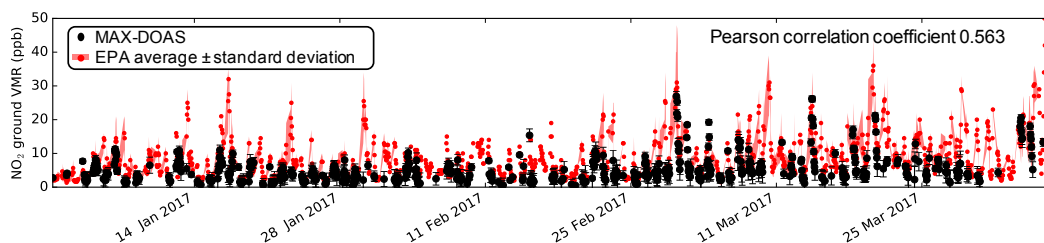


**Figure 6.** Time series comparison of MAX-DOAS-measured NO<sub>2</sub> VMR in the lowest retrieval layer at Broadmeadows (black) vs. average NO<sub>2</sub> for the four Melbourne EPA monitoring sites (red). All measurements are hourly averages during daylight hours only.

pendent variables. In this case  $RV$  ( $V_{\text{MAXDOAS}}/V_{\text{MODIS}}$ ) was 0.37 and the regression analysis showed a slope of 2.18 and Pearson's  $R$  coefficient of 0.33. Therefore, while the ranges for MODIS, averaged over a 10 km spatial radius around Broadmeadows, and MAX-DOAS AOD were very similar (AOD varying between 0.05 and 0.2), the MAX-DOAS AOD was typically half the MODIS-retrieved AOD. Addressing such discrepancies between ground- and satellite-based retrievals is an important ongoing research area, with longer sampling periods and local compatible ceilometer, lidar or PM<sub>2.5</sub> measurements needed for a confident validation of the MAX-DOAS aerosol results.

While no external data for HONO were available in Melbourne, the Victorian Environment Protection Agency (EPA) monitors NO<sub>2</sub> mixing ratios at four sites in the Melbourne metropolitan area (Footscray, Alphington, Dandenong and Altona North, as shown in Fig. 1). The EPA monitors are gas-phase chemiluminescence analysers with molybdenum converters for detection of NO<sub>2</sub>, nitric oxide (NO) and total oxides of nitrogen (NO<sub>x</sub>). As shown in the time series in Fig. 6 several spikes in the average EPA levels are captured by the MAX-DOAS, such as on 4 and 6 January as well as on 1, 2, 4 and 15 March. The Deming regression analysis, with  $RV = 1.25$ , showed a Pearson's  $R$  coefficient of 0.58 and slope of 1.66. The slope of the linear regression highlights that the EPA values are typically higher, which might be expected given that the EPA instruments measure in situ ground level NO<sub>2</sub> while the MAX-DOAS ground volume mixing ratio (VMR) in fact samples the lowest 200 m of the troposphere through which the surface concentration is diluted. Furthermore, given the wide spatial range of the four EPA measurement sites and the possibility for widely varying local sources and meteorological conditions at each site, the observed correlation is a positive result for this comparison. When the local wind direction at Broadmeadows was from the south-west, the correlation for NO<sub>2</sub> between the MAX-DOAS and EPA stations directly to the south-west (Altona North and Footscray) improved to 0.66 (although no change in regression slope was observed), a result which provides the strongest external validation available for these the MAX-DOAS trace gas retrievals.

### 3.3 Source distribution of aerosols, NO<sub>2</sub> and HONO

Combining MAX-DOAS measurements of aerosols and trace gases with co-located meteorological observations allows analysis of spatial source patterns as well as vertical distributions. This is demonstrated using polar bivariate plots where the average trace gas concentrations (Fig. 7a and b) and aerosol extinction (Fig. 7c) are plotted as a function of wind speed and direction. While this method is not a spatial reconstruction, it allows estimation of the main pollution sources given that low wind speed corresponds to localised source regions and high wind speed to pollution transported from further afield. Aerosol extinction, HONO and NO<sub>2</sub> typically show spatially correlated pollution maxima at low wind speed from the southerly and easterly directions. Using the local map in Fig. 7 as a guide, we conclude that the major pollution sources are likely to be the Western Ring Road to the south; the busy Camp Road, Sydney Road and Ring Road intersection to the east; and further to the east Victoria's busiest interstate highway, the Hume Freeway. These results confirm that pollution is being measured by the MAX-DOAS from the expected sectors. High HONO concentration periods are more strongly influenced by both wind direction and speed than NO<sub>2</sub>, suggesting that the HONO source is more strongly localised.

The plots in Fig. 7 are also broken down into weekdays and weekends, showing that weekend NO<sub>2</sub> decreases due to lighter traffic are much more pronounced than for HONO. In fact, during March 2017, the most polluted month of the measurement period, the NO<sub>2</sub> average daily VMR halved from 12 ppb during the week to 6 ppb on the weekend, while the HONO average daily VMR fell only from 0.20 to 0.18 ppb. A similar phenomenon was found by Pusede et al. (2015) in Pasadena, USA, suggesting that correlations and ratios of NO<sub>2</sub> to HONO need to be treated with caution when interpreting potential HONO sources.

Surprisingly, localised aerosol sources do not decrease on weekends, and there is an overall increase in aerosol extinction from the north-east sector. This suggests aerosol extinction could be influenced by longer range transport, including recycling of pollutants around the Melbourne metropolitan area (e.g. Pearce et al., 2011), although it is unclear why such

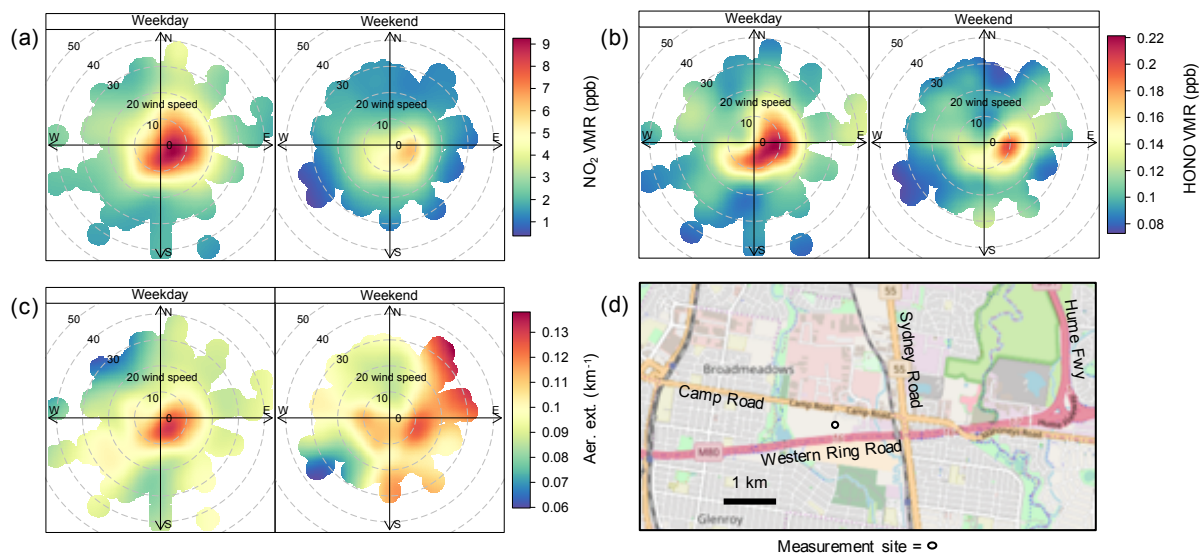


**Figure 7.** (a) Polar bivariate plot for average weekday (left) and weekend (right) NO<sub>2</sub> surface concentration as a function of wind speed and direction. (b) same as (a) but for HONO, (c) same as (a) but for aerosol extinction and (d) map indicating the location of the major road corridors near the measurement site.

an effect would result in pronounced aerosol levels on weekends. It is interesting to note that, while time series and vertical distributions of NO<sub>2</sub> and aerosol extinction are strongly correlated, the differences observed in the spatial distribution provide good evidence that there is no cross correlation in their retrieval.

### 3.4 Periods of elevated HONO levels

During the 3-month measurement period, 33 days which were mostly sunny had peak HONO concentrations in the lowest retrieval layer greater than 0.2 ppb. From the measurement time series (see example time series, Fig. S3 in the Supplement), characteristic ranges for concentration in the lowest retrieval layer were found to be 0 to 0.35 km<sup>-1</sup> for aerosol extinction, 0 to 30 ppb for NO<sub>2</sub> and 0 to 0.5 ppb for HONO. These values for HONO lie within the range of observed VMRs in urban areas around the world (see Table S2 in the Supplement). To further understand the evolution of these species close to the surface over the course of the day, diurnal cycles of HONO, NO<sub>2</sub> and aerosol extinction are shown in Fig. 8. It should be noted that, due to increased DOAS fit residuals and consequent profile retrieval errors for solar zenith angles greater than 80°, no data from SZA > 80° are presented. During autumn in Melbourne this corresponds to approximately 30 min after sunrise and 30 min before sunset. The NO<sub>2</sub> diurnal cycle peaks in the early morning, consistent with morning traffic times on the nearby roadways, remaining around 8 ppb throughout the morning before decreasing until the evening traffic period around 17:00 LT. This diurnal cycle suggests minimal overnight accumulation of nitrogen oxides, a factor which may contribute to the very low ob-

served HONO levels in the early morning (Fig. 8b). In other urban studies, HONO during daylight hours typically peaks close to sunrise and, despite higher-than-expected daytime concentrations, decreases across the course of the day. In contrast, the HONO mixing ratio measured here rises from an early morning minimum to a maximum averaging around 220 ppt, 1 h before solar noon. Previously such daytime maxima in the HONO diurnal cycle have only been observed in rural locations for example at a mountain site in Germany (Acker et al., 2006), a forested site in Michigan, USA (Zhou et al., 2011), and in rural Cyprus (Meusel et al., 2016). In each case, however, the maximum HONO VMR observed was less than in Melbourne, at 110 ppt, 70 and 100 pptv respectively. Therefore, the diurnal maximum HONO measured here is unusual for an urban environment and supports the presence of a strong daytime source.

The HONO/NO<sub>2</sub> ratio has been used previously to categorise emission sources of HONO, with HONO/NO<sub>2</sub> < 0.01 indicating direct emission dominates HONO production (Wojtal et al., 2011; Hendrick et al., 2014; Qin and Mitchell, 2009; Elshorbany et al., 2009). Given that the HONO/NO<sub>2</sub> ratio is consistently greater than 0.01, it is inferred that the observed HONO cannot be attributed to direct traffic emissions from the adjacent road corridors. The magnitude of the midday HONO/NO<sub>2</sub> ratio is more consistent with those measured in Cyprus (Meusel et al., 2016) and rural southern China (Li et al., 2012) than urban Beijing (Hendrick et al., 2014), bearing in mind that average peak NO<sub>2</sub> in summer in Beijing is about double that measured here for Melbourne. In fact, while NO<sub>2</sub> levels are low compared to many urban centres around the world, midday HONO concentrations and HONO/NO<sub>2</sub> ratios here are comparable with midday levels

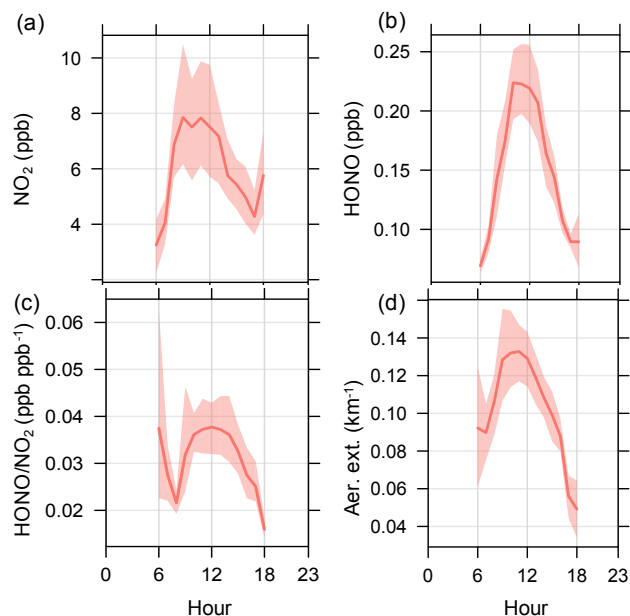


**Figure 8.** Data from 33 days in the measurement period with high daytime peak HONO. Diurnal cycle plots for the 1-hourly averages of (a) NO<sub>2</sub>, (b) HONO, (c) HONO/NO<sub>2</sub> and (d) aerosol extinction surface values at Broadmeadows. Solid line shows average values; shaded areas are 95 % confidence intervals.

reported in Beijing, China (Hendrick et al., 2014); London, UK (Lee et al., 2016); and Pasadena (Pusede et al., 2015) and Houston (Wong et al., 2012), USA (see also Table S2 in the Supplement for a comparison of urban HONO and NO<sub>2</sub> observations from around the world).

The implication of the high daytime HONO levels for the tropospheric oxidation capacity was assessed by comparing the OH radical production rates from HONO photolysis (Reaction R3) and ozone photolysis (Reactions R1, R2). These are given respectively by

$$\begin{aligned} P(\text{OH})_{\text{O}_3} &= 2 \times f \times J(\text{O}^1\text{D}) \times [\text{O}_3], \\ P(\text{OH})_{\text{HONO}} &= J(\text{HONO}) \times [\text{HONO}]. \end{aligned} \quad (3)$$

In Eq. (3),  $f$  is the fraction of O<sup>1</sup>D reacting with water vapour to form OH (Finlayson-Pitts and Pitts Jr., 1999). [O<sub>3</sub>] is the ozone concentration in ppb, which was taken from averaged EPA measurements of surface ozone concentration around Melbourne, and [HONO] is the VMR in the lowest retrieval layer in ppb, from the MAX-DOAS retrieval. The photolysis rates  $J(\text{O}^1\text{D})$  and  $J(\text{HONO})$  were calculated using the Tropospheric Ultraviolet and Visible (TUV) radiation model (Madronich and Flocke, 1999). Photolysis rates were simulated for 7 March 2017, a clear sunny day with a HONO midday peak of 400 ppt and a Melbourne EPA average O<sub>3</sub> surface concentration of 27 ppb. The aerosol optical depth was fixed at 0.15 (from the MAX-DOAS aerosol retrieval), and the total ozone column was fixed at 270 DU,

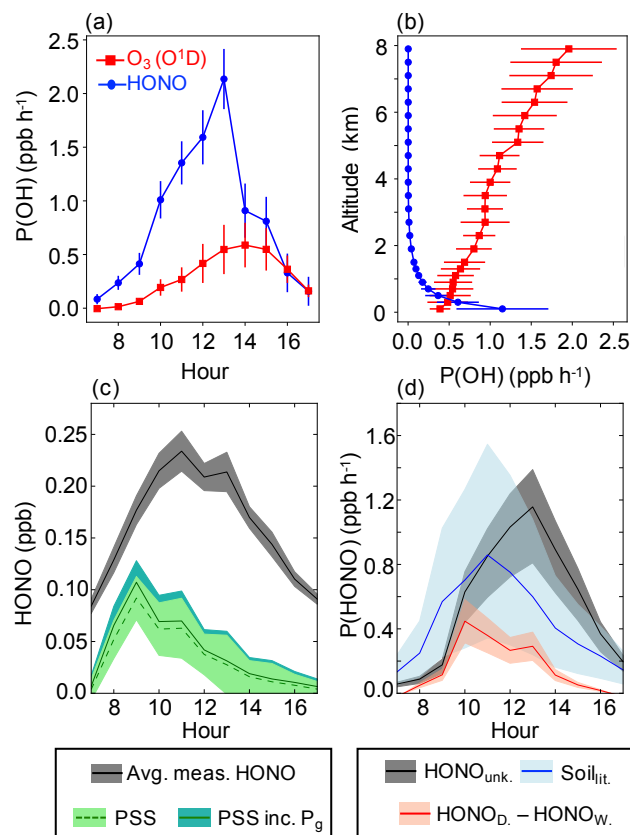


**Figure 9.** (a) Diurnal cycle of ground level OH radical production  $P(\text{OH})$  from ozone (O<sub>3</sub> to O<sup>1</sup>D) and HONO photolysis, calculated for an example day with 27 ppb surface ozone, and the HONO diurnal cycle from 7 March 2018 which peaked near midday at around 400 ppt. (b) Vertical profiles of tropospheric OH radical production from HONO photolysis, calculated using the average measured HONO vertical profile and from ozone photolysis calculated using co-located ozone sonde data averaged from January to April 2018. Points represent the mean; error bars represent 1 standard deviation. (c) Measured average HONO diurnal cycle plotted with the calculated photostationary state (PSS) HONO concentration and PSS including the NO<sub>2</sub> ground conversion term (PSS including  $P_g$ ). (d) HONO<sub>unk.</sub> is the unknown HONO production rate (measured minus PSS), HONO<sub>D</sub> – HONO<sub>W</sub> is the measured HONO emission rate attributable to soil processes (driest conditions minus wettest conditions, see Fig. 11 and discussion in Sect. 3.5), and Soil<sub>lit.</sub> represents PSS and literature HONO and NO soil emission rates. Lines represent means; shaded regions represent 95 % confidence intervals.

consistent with zenith DOAS measurements using the same MAX-DOAS instrument. The TUV simulated  $J(\text{O}^1\text{D})$  values were consistent with the empirical parameterisation of Wilson (2015) for  $J(\text{O}^1\text{D})$  at Cape Grim in north-western Tasmania. The resulting  $P(\text{OH})$  diurnal values are presented in Fig. 9a, showing that the peak OH production rate in the middle of the day was estimated at 0.5 ppb h<sup>-1</sup> from O<sub>3</sub> photolysis, and on 7 March it was around 2 ppb h<sup>-1</sup> from HONO

photolysis. Note that since the HONO mixing ratios are calculated throughout the lowest retrieval layer (0–200 m) the ground surface mixing ratios, and therefore the OH production rates, are likely to be larger. This suggests that HONO levels at 400 ppt in the middle of the day can increase the local OH radical production by up to a factor of 4, significantly increasing the local tropospheric oxidative capacity in Melbourne. For the 33 days with high daytime HONO peaks, the average diurnal cycle peak of [HONO] at 220 ppt corresponds to a source of OH radicals around 1 ppb h<sup>-1</sup>, double that from ozone photolysis.

HONO has previously been observed to be the dominant primary OH production mechanism in urban areas (e.g. Ren et al., 2003; Elshorbany et al., 2009) using in situ measurements and modelling of surface mixing ratios. Given that the MAX-DOAS technique provides vertical profiles of HONO, the calculation of vertical OH production profiles due to HONO photolysis is possible. With co-located ozone sonde measurements at the Broadmeadows site, primary OH production has been compared across the lowest 8 km of the troposphere in Fig. 9b. Ozone sonde data have been averaged across all measurements (17 midday measurements, approximately weekly) during the MAX-DOAS measurement period (21 December 2016 to 7 April 2017) and included temperature, pressure and relative humidity, which enabled water mixing ratios to be estimated throughout the troposphere. The resulting vertical OH production profile due to O<sub>3</sub> is compared with that expected from the average midday HONO profile throughout the campaign, assuming that no extra HONO sources existed above the MAX-DOAS top retrieval height (4 km). Figure 9b shows that, while OH production is dominated close to the ground by HONO photolysis, ozone photolysis is dominant above 1 km and will therefore be the dominant OH radical source throughout the whole troposphere. This demonstrates that considering only surface values can give a distorted picture of the relative importance of different radical sources and highlights the ability of the MAX-DOAS technique to provide important vertically resolved information on tropospheric oxidation chemistry.

### 3.5 Possible daytime HONO sources

The HONO diurnal profile observed in this campaign matches temporally with the diurnal profile of the missing HONO production source calculated in both rural (e.g. Meusel et al., 2016) and urban areas (e.g. Wong et al., 2012; Pusede et al., 2015). In order to determine the magnitude of the unknown HONO concentration in Melbourne, a simple photostationary state (PSS) calculation has been performed following the example of Kleffmann (2007).

$$[\text{HONO}]_{\text{PSS}} = \frac{k_1[\text{OH}][\text{NO}] + P_g}{k_2[\text{OH}] + J(\text{HONO})} \quad (4)$$

The temperature-dependent rate constants  $k_1$  and  $k_2$  are for Reactions (R4) and (R6) respectively and have been cal-

culated according to the parameterisations in Atkinson et al. (2004). Unfortunately, no hydroxyl radical (OH) or nitric oxide (NO) measurements were available at the measurement location during the campaign. To enable a PSS estimate, OH concentrations have been estimated using a simple box model which has been initialised using pollutant emissions data from Sydney in the absence of up-to-date emissions data for Melbourne. Simulated OH radical concentrations peaked at 0.07 ppt in the middle of the day in good agreement with measured background OH levels at Cape Grim in north-western Tasmania, to the south of Melbourne (Creasey et al., 2003). NO concentrations are measured by the Victorian EPA in conjunction with NO<sub>2</sub> at four monitoring sites around metropolitan Melbourne, and from these NO and NO<sub>2</sub> measurements an average diurnally varying NO/NO<sub>2</sub> ratio was calculated. The local NO concentration at the MAX-DOAS measurement site was then estimated as  $\text{NO}_{\text{local}} = \text{NO}_{2\text{local}} \times (\text{NO}/\text{NO}_2)_{\text{EPA}}$ . As in Michoud et al. (2014), the PSS equation can be expanded from considering only the photochemistry by including additional parameterised HONO source or sink terms in the PSS numerator or denominator respectively. In Eq. (4),  $P_g$  represents an additional source term due to ground conversion of NO<sub>2</sub> where  $P_g = k_c \times 0.25 \times J(\text{NO}_2) \times [\text{NO}_2]$  and  $0.25 \times J(\text{NO}_2)$  is the scaled NO<sub>2</sub> photolysis rate calculated using the TUV model (Lee et al., 2016). The ground conversion rate  $k_c$  has been set to  $6 \times 10^{-6}$ , which was found in Lee et al. (2016) to be the average ground conversion rate necessary to close the missing HONO budget in London. As seen in Fig. 9c, the calculated HONO PSS concentration underestimates HONO levels especially in the middle of the day and the afternoon, consistent with previous observations in both rural (e.g. Meusel et al., 2016) and urban (e.g. Michoud et al., 2014; Lee et al., 2016) environments.

HONO and NO<sub>2</sub> mixing ratios are strongly correlated (Pearson's  $R = 0.81$ ) in the lowest retrieval layer as shown in Fig. 10. The Pearson's  $R$  coefficient decreases with increasing altitude (see Table S3 in the Supplement), which could indicate that conversion of NO<sub>2</sub> at the ground level is contributing to the observed HONO. However, caution should be taken in interpreting this result since the shorter lifetime and hence expected stronger vertical gradient of HONO compared to NO<sub>2</sub> would also lead to a decreasing correlation with altitude. Furthermore, given that the PSS calculation includes the strong NO<sub>2</sub> ground conversion rate in Lee et al. (2016) and still cannot replicate the average HONO diurnal profile, photolytic ground NO<sub>2</sub> conversion cannot be the dominant daytime HONO source in Melbourne. The heterogeneous conversion of NO<sub>2</sub> on wet surfaces according to Reaction (R5) has been suggested as a primary HONO source pathway (Wong et al., 2012) especially during the night when there are no OH radicals available to form HONO via Reaction (R4). However, while Fig. 10b shows that most of the data points for HONO/NO<sub>2</sub> > 0.025 correspond to relative humidity less than 50 %, there is no clear trend for

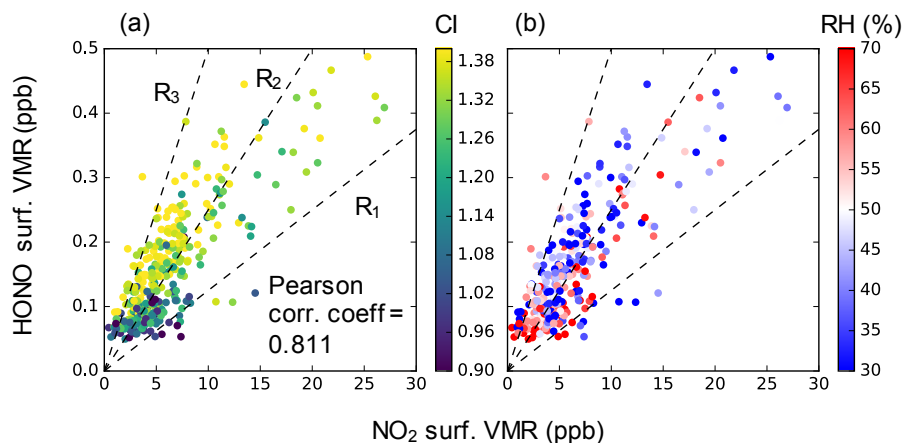


**Figure 10.** Scatter plots of (a) HONO ground concentration vs. NO<sub>2</sub> ground concentration coloured by colour index (CI), showing dependence of high HONO values on solar radiation. Note that CI is the ratio of intensities measured by the MAX-DOAS instrument at 330 and 390 nm. The cloud-filtered CI correlated strongly with global irradiance measured 6 km to the west at Melbourne Airport. (b) HONO ground concentration vs. NO<sub>2</sub> ground concentration coloured by relative humidity. Dashed lines represent the ratios  $R_1$  HONO/NO<sub>2</sub> = 0.0125,  $R_2$  HONO/NO<sub>2</sub> = 0.025 and  $R_3$  HONO/NO<sub>2</sub> = 0.05.

HONO/NO<sub>2</sub> < 0.025. Regression analysis showed that the overall correlation between relative humidity and HONO VMR was very weak (slope  $-0.001$ , Pearson's  $R$  coefficient  $-0.16$ ), further indicating that Reaction (R5) cannot explain the high daytime HONO.

Photo-enhanced uptake and conversion of NO<sub>2</sub> on aerosols, such as organics, has been proposed as a daytime HONO source (e.g. George et al., 2005). Only moderate temporal correlations of Pearson's  $R = 0.58$  and  $0.49$  between aerosols and HONO were found for surface and total column amounts respectively. In addition, HONO and aerosol vertical distributions were often different as indicated in Figs. 4 and 5, indicating that aerosol-mediated NO<sub>2</sub> conversion cannot explain the observed high daytime HONO levels. This is in line with previous findings in for example Michoud et al. (2014) and Lee et al. (2016). Therefore, while plausible photoactivated, ground-based NO<sub>2</sub> conversion mechanisms exist, such mechanisms are either saturated and/or of insufficient strength to account for the observed daytime HONO.

Therefore, other mechanisms, independent of NO<sub>2</sub>, may be contributing to the daytime HONO formation. Processes at the ground surface have been suggested to provide strong daytime HONO sources, including nighttime deposition of HONO or gaseous atmospheric acids to a surface reservoir followed by daytime re-emission (VandenBoer et al., 2014, 2015), as well as photoactivated reactions involving humic acids (Stemmler et al., 2006) and soil nitrites (Su et al., 2011). Such ground-based sources match both the strong vertical HONO gradients and diurnal profile of the daytime HONO observed in Melbourne, suggesting that these mechanisms could explain the presence of HONO in the middle of the day. Lee et al. (2016) concluded that, in London, the highly urbanised environment surrounding the measurement

site meant soil-based HONO contributions were unlikely to contribute to the observed high daytime HONO budget. In contrast, since the Broadmeadows measurement site is surrounded by a variety of surfaces including vacant fields, wide grassed road verges, medium-density outer-suburban development and parkland, consequently soil-based processes must be considered in the possible daytime HONO formation mechanisms.

Meusel et al. (2018) showed that, in Cyprus, emissions from soil and soil biocrusts could maximally explain 85 % of the local daytime missing HONO source. Measurements of reactive nitrogen fluxes from bacteria in soil biocrusts by Weber et al. (2015) and Meusel et al. (2018) found that optimum HONO and NO emission conditions were between 20 and 40 % soil water content (SWC), while Oswald et al. (2013) showed that maximum reactive nitrogen flux from a range of soil samples around the world occurred at around 10 % SWC. In order to test the potential role of soil emissions on the HONO budget in Melbourne, modelled soil moisture data have been obtained from the Australian Water Resources Assessment Modelling System (Hafeez et al., 2015). Figure 11 shows a clear variation in midday HONO and NO<sub>2</sub> levels with soil moisture, suggesting that reactive nitrogen emissions from the soil may be a key factor in both HONO and NO levels. HONO and NO<sub>2</sub> levels are observed to decrease above 10 % SWC, below the optimum SWC for reactive nitrogen emissions from biocrusts (Meusel et al., 2018, and Weber et al., 2015) but consistent with the optimum conditions for soil samples in Oswald et al. (2013).

The soil-mediated HONO production rate in  $\text{ppb h}^{-1}$  could be estimated by looking at the difference between the production rates in the driest and wettest SWC bins, as shown in red in Fig. 9d. This rate closes the HONO budget in the

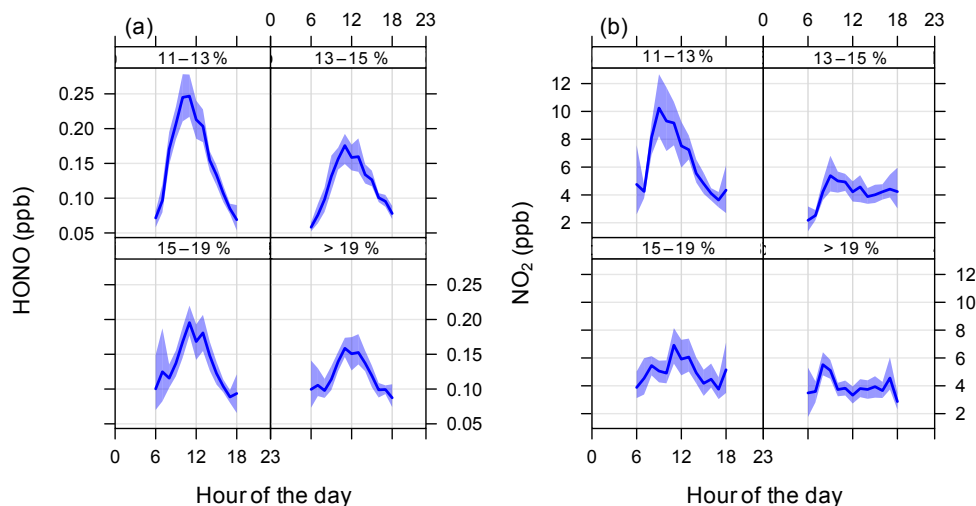


**Figure 11.** (a) HONO and (b) NO<sub>2</sub> diurnal cycles over the 3-month measurement period, divided into four soil water content (SWC) % bins. SWC data have been obtained from the Australian Water Resources Assessment Modelling System.

morning but not in the middle of the day or afternoon. To test whether soil-based processes could close the whole budget, an updated HONO<sub>PSS</sub> has been calculated by including the diurnal cycle of soil HONO and NO soil emissions from Cyprus, presented in Meusel et al. (2018). Shown in blue in Fig. 9d, large shaded error margins on this plot indicate the wide range of observed HONO and NO fluxes from the Cyprus samples. Comparison with Melbourne is complicated by the dependence of HONO and NO fluxes on a wide variety of other soil parameters outside the scope of this study, including soil properties, pH and temperature. Nevertheless, the comparison suggests that soil emissions have the potential to bridge the midday and afternoon gap in the HONO production rate, providing strong evidence that it would be worthwhile to investigate soil-based reactive nitrogen emissions in Melbourne.

#### 4 Conclusions

Here we report on the first MAX-DOAS measurements from Melbourne, Australia (37.7° S, 144.9° E), from December 2016 to November 2017. A detailed uncertainty analysis of the retrieval a priori and aerosol parameters, combined with HONO DOAS fitting window optimisation, provides confidence in retrievals of aerosol extinction, NO<sub>2</sub> and HONO using the HEIPRO algorithm. The NO<sub>2</sub> results are comparable to the EPA air quality monitoring carried out around Melbourne, with average maximum NO<sub>2</sub> at 8 ppb. Despite the moderate to low NO<sub>2</sub> pollution levels, high daytime HONO was commonly recorded with peak values in the late morning around 220 ppt. Such a consistent daytime HONO diurnal peak has previously been reported only in rural areas and matches previously calculated diurnal profiles for a HONO

missing source, which was found here to have a production rate 1 ppb h<sup>-1</sup> above the photostationary state HONO concentration. While strong vertical and temporal correlations between HONO and NO<sub>2</sub> exist generally, the correlation does not hold between weekends and weekdays and ground-based NO<sub>2</sub> conversion rates are insufficient to bridge the midday unknown HONO source gap. Strong relationships between solar radiation and HONO and strong HONO vertical gradients support previous theories that the missing HONO source is photolytically activated and ground based. Furthermore, a dependence of both NO<sub>2</sub> and HONO on soil moisture content suggests that soil emissions may be playing an important role in the local reactive nitrogen chemistry. These findings suggest that HONO is significantly increasing the local tropospheric oxidation capacity, with an OH radical source strength up to 4 times stronger in the lowest 500 m of the troposphere than from ozone photolysis. Future studies in the Melbourne area should explore the oxidative cycles of HONO and OH involving soil processes. Through analysis of oxidation processes involving volatile organic compounds and ozone, in addition the reactive nitrogen cycle, future studies using MAX-DOAS should work towards a more complete understanding of vertical, spatial and temporal variations in tropospheric oxidation chemistry.

*Data availability.* MAX-DOAS data from the Bureau of Meteorology (BOM) Broadmeadows site are available upon request to Steve Rhodes (steve.rhodes@bom.gov.au). Meteorological data for Melbourne are available via BOM data services online (<http://www.bom.gov.au/climate/data-services>, Australian Bureau of Meteorology, 2018). Vertical ozone profile data are available via the World Ozone and Ultraviolet Radiation Data Centre (<https://woudc.org>, Meteorological Service of Canada, 2018). Air quality data for

Melbourne are available via the Victorian Environment Protection Agency website (<https://www.epa.vic.gov.au>, Environment Protection Agency Victoria, 2018).

**The Supplement related to this article is available online at <https://doi.org/10.5194/acp-18-13969-2018-supplement>.**

*Author contributions.* SR and MT maintained the MAX-DOAS instrument collecting the data. RGR conducted the data analysis and drafted the manuscript. RGR, SW, NJ, UF and RS contributed to developing the scientific direction, analysis protocols and writing the manuscript.

*Competing interests.* The authors declare that they have no conflict of interest.

*Acknowledgements.* RGR wishes to acknowledge helpful discussions with Peter Rayner on atmospheric inverse methods and Johannes Lampel on DOAS fitting methods, as well as Paul Torre and the Victorian Environment Protection Agency for making air quality data available. The authors acknowledge Thomas Danckert, Caroline Fayt and Michel van Roozendaal, authors of the QDOAS software used in DOAS analysis in this work. RS and RGR acknowledge support from the Australian Research Council's Centre of Excellence for Climate System Science (CE110001028) and the Australian Research Council's Discovery project: Tackling Atmospheric Chemistry Grand Challenges in the Southern Hemisphere (DP160101598).

Edited by: Robert McLaren

Reviewed by: two anonymous referees

## References

- AccessEconomics: The health of nations: the value of a statistical life, Tech. rep., Office of the Australian Safety and Compensation Council, 2008.
- Acker, K. and Möller, D.: Atmospheric variation of nitrous acid at different sites in Europe, *Environ. Chem.*, 4, 242–255, 1449–8979, 2007.
- Acker, K., Moller, D., Wieprecht, W., Meixner, F. X., Bohn, B., Gilge, S., Plass-Dülmer C., and Berresheim, H.: Strong daytime production of OH from HNO<sub>2</sub> at a rural mountain site, *Geophys. Res. Lett.*, 33, L02809, <https://doi.org/10.1029/2005GL024643>, 2006.
- Atkinson, R., Baulch, D. L., Cox, R. A., Crowley, J. N., Hampson, R. F., Hynes, R. G., Jenkin, M. E., Rossi, M. J., and Troe, J.: Evaluated kinetic and photochemical data for atmospheric chemistry: Volume I – gas phase reactions of O<sub>x</sub>, HO<sub>x</sub>, NO<sub>x</sub> and SO<sub>x</sub> species, *Atmos. Chem. Phys.*, 4, 1461–1738, <https://doi.org/10.5194/acp-4-1461-2004>, 2004.
- Australian Bureau of Meteorology: Climate data online, <http://www.bom.gov.au/climate/data>, last access: 1 April 2018.
- Barnett, A. G., Williams, G. M., Schwartz, J., Best, T. L., Neller, A. H., Petroeschovsky, A. L., and Simpson, R. W.: The effects of air pollution on hospitalizations for cardiovascular disease in elderly people in Australian and New Zealand cities, *Environ. Health Perspect.*, 114, 1018, <https://doi.org/10.1289/ehp.8674>, 2006.
- Begg, S., Vos, T., Barker, B., Stevenson, C., Stanley, L., and Lopez, A. D.: The burden of disease and injury in Australia 2003, Tech. rep., Australian Institute of Health and Welfare, 2007.
- Creasey, D., Evans, G., Heard, D., and Lee, J.: Measurements of OH and HO<sub>2</sub> concentrations in the Southern Ocean marine boundary layer, *J. Geophys. Res.-Atmos.*, 108, 4475, <https://doi.org/10.1029/2002JD003206>, 2003.
- Elshorbany, Y. F., Kurtenbach, R., Wiesen, P., Lissi, E., Rubio, M., Villena, G., Gramsch, E., Rickard, A. R., Pilling, M. J., and Kleffmann, J.: Oxidation capacity of the city air of Santiago, Chile, *Atmos. Chem. Phys.*, 9, 2257–2273, <https://doi.org/10.5194/acp-9-2257-2009>, 2009.
- Environment Protection Agency Victoria: Historic Air Quality Data Table, <https://www.epa.vic.gov.au>, last access: 1 April 2018.
- EPA, V.: Future air quality in Victoria Future air quality in Victoria – Final report, Tech. rep., Environmental Protection Agency Victoria, 2013.
- Feister, U. and Grewe, R.: Spectral albedo measurements in the UV and visible region over different types of surfaces, *Photochem. Photobiol.*, 62, 736–744, 1995.
- Finlayson-Pitts, B. J. and Pitts Jr., J. N.: Chemistry of the upper and lower atmosphere: theory, experiments, and applications, Academic Press, San Diego, CA, USA, 1999.
- Frieß, U., Monks, P. S., Remedios, J. J., Rozanov, A., Sinreich, R., Wagner, T., and Platt, U.: MAX-DOAS O<sub>4</sub> measurements: A new technique to derive information on atmospheric aerosols: 2. Modeling studies, *J. Geophys. Res.-Atmos.*, 111, D14203, <https://doi.org/10.1029/2005JD006618>, 2006.
- Garcia-Nieto, D., Benavent, N., and Saiz-Lopez, A.: Measurements of atmospheric HONO vertical distribution and temporal evolution in Madrid (Spain) using the MAX-DOAS technique, *Sci. Total Environ.*, 643, 957–966, <https://doi.org/10.1016/j.scitotenv.2018.06.180>, 2018.
- George, C., Strekowski, R., Kleffmann, J., Stemmler, K., and Ammann, M.: Photoenhanced uptake of gaseous NO<sub>2</sub> on solid organic compounds: a photochemical source of HONO?, *Faraday Discuss.*, 130, 195–210, 2005.
- Hafeez, F., Frost, A., Vaze, J., Dutta, D., Smith, A., and Elmahdi, A.: A new integrated continental hydrological simulation system, *Water: Journal of the Australian Water Association*, 42, 75–82, 2015.
- Hendrick, F., Müller, J.-F., Clémer, K., Wang, P., De Mazière, M., Fayt, C., Gielen, C., Hermans, C., Ma, J. Z., Pinardi, G., Stavrou, T., Vlemmix, T., and Van Roozendaal, M.: Four years of ground-based MAX-DOAS observations of HONO and NO<sub>2</sub> in the Beijing area, *Atmos. Chem. Phys.*, 14, 765–781, <https://doi.org/10.5194/acp-14-765-2014>, 2014.
- Hermans, C., Vandaele, A., Fally, S., Carleer, M., Colin, R., Coquart, B., Jenouvrier, A., and Merienne, M.-F.: Absorption cross-section of the collision-induced bands of oxygen from the UV to the NIR, 193–202, Springer, 2003.
- Hönninger, G., von Friedeburg, C., and Platt, U.: Multi axis differential optical absorption spectroscopy (MAX-DOAS), *At-*

- mos. Chem. Phys., 4, 231–254, <https://doi.org/10.5194/acp-4-231-2004>, 2004.
- Huang, R.-J., Yang, L., Cao, J., Wang, Q., Tie, X., Ho, K.-F., Shen, Z., Zhang, R., Li, G., and Zhu, C.: Concentration and sources of atmospheric nitrous acid (HONO) at an urban site in Western China, *Sci. Total Environ.*, 593, 165–172, 2017.
- Jin, J., Ma, J., Lin, W., Zhao, H., Shaiganfar, R., Beirle, S., and Wagner, T.: MAX-DOAS measurements and satellite validation of tropospheric NO<sub>2</sub> and SO<sub>2</sub> vertical column densities at a rural site of North China, *Atmos. Environ.*, 133, 12–25, 2016.
- Kanaya, Y., Irie, H., Takashima, H., Iwabuchi, H., Akimoto, H., Sudo, K., Gu, M., Chong, J., Kim, Y. J., Lee, H., Li, A., Si, F., Xu, J., Xie, P.-H., Liu, W.-Q., Dzhola, A., Postlyakov, O., Ivanov, V., Grechko, E., Terpugova, S., and Panchenko, M.: Long-term MAX-DOAS network observations of NO<sub>2</sub> in Russia and Asia (MADRAS) during the period 2007–2012: instrumentation, elucidation of climatology, and comparisons with OMI satellite observations and global model simulations, *Atmos. Chem. Phys.*, 14, 7909–7927, <https://doi.org/10.5194/acp-14-7909-2014>, 2014.
- Kleffmann, J.: Daytime sources of nitrous acid (HONO) in the atmospheric boundary layer, *Chem. Phys. Chem.*, 8, 1137–1144, 2007.
- Kleffmann, J., Kurtenbach, R., Lörzer, J., Wiesen, P., Kalthoff, N., Vogel, B., and Vogel, H.: Measured and simulated vertical profiles of nitrous acid—Part I: Field measurements, *Atmos. Environ.*, 37, 2949–2955, 1352–2310, 2003.
- Kleffmann, J., Lörzer, J., Wiesen, P., Kern, C., Trick, S., Volkamer, R., Rodenas, M., and Wirtz, K.: Intercomparison of the DOAS and LOPAP techniques for the detection of nitrous acid (HONO), *Atmos. Environ.*, 40, 3640–3652, 2006.
- Lampel, J., Frieß, U., and Platt, U.: The impact of vibrational Raman scattering of air on DOAS measurements of atmospheric trace gases, *Atmos. Meas. Tech.*, 8, 3767–3787, <https://doi.org/10.5194/amt-8-3767-2015>, 2015.
- Lampel, J., Pöhler, D., Polyansky, O. L., Kyuberis, A. A., Zobov, N. F., Tennyson, J., Lodi, L., Frieß, U., Wang, Y., Beirle, S., Platt, U., and Wagner, T.: Detection of water vapour absorption around 363 nm in measured atmospheric absorption spectra and its effect on DOAS evaluations, *Atmos. Chem. Phys.*, 17, 1271–1295, <https://doi.org/10.5194/acp-17-1271-2017>, 2017.
- Lee, J. D., Whalley, L. K., Heard, D. E., Stone, D., Dunmore, R. E., Hamilton, J. F., Young, D. E., Allan, J. D., Laufs, S., and Kleffmann, J.: Detailed budget analysis of HONO in central London reveals a missing daytime source, *Atmos. Chem. Phys.*, 16, 2747–2764, <https://doi.org/10.5194/acp-16-2747-2016>, 2016.
- Li, X., Brauers, T., Hofzumahaus, A., Lu, K., Li, Y. P., Shao, M., Wagner, T., and Wahner, A.: MAX-DOAS measurements of NO<sub>2</sub>, HCHO and CHOCHO at a rural site in Southern China, *Atmos. Chem. Phys.*, 13, 2133–2151, <https://doi.org/10.5194/acp-13-2133-2013>, 2013.
- Li, X., Brauers, T., Häsel, R., Bohn, B., Fuchs, H., Hofzumahaus, A., Holland, F., Lou, S., Lu, K. D., Rohrer, F., Hu, M., Zeng, L. M., Zhang, Y. H., Garland, R. M., Su, H., Nowak, A., Wiedensohler, A., Takegawa, N., Shao, M., and Wahner, A.: Exploring the atmospheric chemistry of nitrous acid (HONO) at a rural site in Southern China, *Atmos. Chem. Phys.*, 12, 1497–1513, <https://doi.org/10.5194/acp-12-1497-2012>, 2012.
- Li, X., Rohrer, F., Hofzumahaus, A., Brauers, T., Häsel, R., Bohn, B., Broch, S., Fuchs, H., Gomm, S., and Holland, F.: Missing gas-phase source of HONO inferred from Zeppelin measurements in the troposphere, *Science*, 344, 292–296, 2014.
- Ma, J. Z., Beirle, S., Jin, J. L., Shaiganfar, R., Yan, P., and Wagner, T.: Tropospheric NO<sub>2</sub> vertical column densities over Beijing: results of the first three years of ground-based MAX-DOAS measurements (2008–2011) and satellite validation, *Atmos. Chem. Phys.*, 13, 1547–1567, <https://doi.org/10.5194/acp-13-1547-2013>, 2013.
- Madronich, S., and Flocke, S.: The role of solar radiation in atmospheric chemistry, in: *Environmental Photochemistry*, Springer, Berlin, Heidelberg, Germany, 1–26, 1999.
- Meteorological Service of Canada: World Ozone and Ultraviolet Radiation Data Centre, <https://woudc.org>, last access: 1 April 2018.
- Meusel, H., Kuhn, U., Reiffs, A., Mallik, C., Harder, H., Martinez, M., Schuladen, J., Bohn, B., Parchatka, U., Crowley, J. N., Fischer, H., Tomsche, L., Novelli, A., Hoffmann, T., Janssen, R. H. H., Hartogensis, O., Pikridas, M., Vrekoussis, M., Bourtsoukidis, E., Weber, B., Lelieveld, J., Williams, J., Pöschl, U., Cheng, Y., and Su, H.: Daytime formation of nitrous acid at a coastal remote site in Cyprus indicating a common ground source of atmospheric HONO and NO, *Atmos. Chem. Phys.*, 16, 14475–14493, <https://doi.org/10.5194/acp-16-14475-2016>, 2016.
- Meusel, H., Tamm, A., Kuhn, U., Wu, D., Leifke, A. L., Fiedler, S., Ruckteschler, N., Yordanova, P., Lang-Yona, N., Pöhlker, M., Lelieveld, J., Hoffmann, T., Pöschl, U., Su, H., Weber, B., and Cheng, Y.: Emission of nitrous acid from soil and biological soil crusts represents an important source of HONO in the remote atmosphere in Cyprus, *Atmos. Chem. Phys.*, 18, 799–813, <https://doi.org/10.5194/acp-18-799-2018>, 2018.
- Michoud, V., Colomb, A., Borbon, A., Miet, K., Beekmann, M., Camredon, M., Aumont, B., Perrier, S., Zapf, P., Siour, G., Ait-Helal, W., Afif, C., Kukui, A., Furger, M., Dupont, J. C., Haefelin, M., and Doussin, J. F.: Study of the unknown HONO daytime source at a European suburban site during the MEGAPOLI summer and winter field campaigns, *Atmos. Chem. Phys.*, 14, 2805–2822, <https://doi.org/10.5194/acp-14-2805-2014>, 2014.
- Neuman, J., Trainer, M., Brown, S., Min, K., Nowak, J., Parrish, D., Peischl, J., Pollack, I., Roberts, J., and Ryerson, T.: HONO emission and production determined from airborne measurements over the Southeast US, *J. Geophys. Res.-Atmos.*, 121, 9237–9250, 2016.
- Ortega, I., Koenig, T., Sinreich, R., Thomson, D., and Volkamer, R.: The CU 2-D-MAX-DOAS instrument – Part 1: Retrieval of 3-D distributions of NO<sub>2</sub> and azimuth-dependent OVOC ratios, *Atmos. Meas. Tech.*, 8, 2371–2395, <https://doi.org/10.5194/amt-8-2371-2015>, 2015.
- Ortega, I., Berg, L. K., Ferrare, R. A., Hair, J. W., Hostetler, C. A., and Volkamer, R.: Elevated aerosol layers modify the O<sub>2</sub>–O<sub>2</sub> absorption measured by ground-based MAX-DOAS, *J. Quant. Spectrosc. Ra.*, 176, 34–49, 2016.
- Oswald, R., Behrendt, T., Ermel, M., Wu, D., Su, H., Cheng, Y., Breuninger, C., Moravek, A., Mougou, E., and Delon, C.: HONO emissions from soil bacteria as a major source of atmospheric reactive nitrogen, *Science*, 341, 1233–1235, 2013.
- Pearce, J. L., Beringer, J., Nicholls, N., Hyndman, R. J., Uotila, P., and Tapper, N. J.: Investigating the influence of synoptic-scale

- meteorology on air quality using self-organizing maps and generalized additive modelling. *Atmos. Environ.*, 45, 128–136, 2011.
- Pinto, J., Dibb, J., Lee, B., Rappengluck, B., Wood, E., Levy, M., Zhang, R.-Y., Lefer, B., Ren, X.-R., and Stutz, J.: Intercomparison of field measurements of nitrous acid (HONO) during the SHARP campaign, *J. Geophys. Res.-Atmos.*, 119, 5583–5601, 2014.
- Platt, U. and Perner, D.: Measurements of atmospheric trace gases by long path differential UV/visible absorption spectroscopy, in: *Optical and Remote Sensing*, Springer, Berlin, Heidelberg, Germany, 97–105, 1983.
- Platt, U. and Stutz, J.: *Differential Optical Absorption Spectroscopy*, Springer-Verlag Berlin Heidelberg, Berlin, 2008.
- Pusede, S. E., VandenBoer, T. C., Murphy, J. G., Markovic, M. Z., Young, C. J., Veres, P. R., Roberts, J. M., Washenfelder, R. A., Brown, S. S., and Ren, X.: An atmospheric constraint on the NO<sub>2</sub> dependence of daytime near-surface nitrous acid (HONO), *Environ. Sci. Technol.*, 49, 12774–12781, 2015.
- Qin, M., Xie, P., Su, H., Gu, J., Peng, F., Li, S., Zeng, L., Liu, J., Liu, W., and Zhang, Y.: An observational study of the HONO–NO<sub>2</sub> coupling at an urban site in Guangzhou City, South China, *Atmos. Environ.*, 43, 5731–5742, 2009.
- Qin, Y. and Mitchell, R. M.: Characterisation of episodic aerosol types over the Australian continent, *Atmos. Chem. Phys.*, 9, 1943–1956, <https://doi.org/10.5194/acp-9-1943-2009>, 2009.
- Ren, X., Harder, H., Martinez, M., Leshner, R. L., Olinger, A., Simpasa, J. B., Brune, W. H., Schwab, J. J., Demerjian, K. L., and He, Y.: OH and HO<sub>2</sub> chemistry in the urban atmosphere of New York City, *Atmos. Environ.*, 37, 3639–3651, 2003.
- Rodgers, C. D.: Characterization and error analysis of profiles retrieved from remote sounding measurements, *J. Geophys. Res.-Atmos.*, 95, 5587–5595, 1990.
- Rodgers, C. D.: *Inverse methods for atmospheric sounding: theory and practice*, vol. 2, World scientific, Singapore, 2000.
- Roscoe, H. K., Van Roozendaal, M., Fayt, C., du Piesanie, A., Abuhassan, N., Adams, C., Akrami, M., Cede, A., Chong, J., Clémer, K., Friess, U., Gil Ojeda, M., Goutail, F., Graves, R., Griesfeller, A., Grossmann, K., Hemerijckx, G., Hendrick, F., Herman, J., Hermans, C., Irie, H., Johnston, P. V., Kanaya, Y., Kreher, K., Leigh, R., Merlaud, A., Mount, G. H., Navarro, M., Oetjen, H., Pazmino, A., Perez-Camacho, M., Peters, E., Pinardi, G., Puentedura, O., Richter, A., Schönhardt, A., Shaiganfar, R., Spinei, E., Strong, K., Takashima, H., Vlemmix, T., Vrekoussis, M., Wagner, T., Wittrock, F., Yela, M., Yilmaz, S., Boersma, F., Hains, J., Kroon, M., Piters, A., and Kim, Y. J.: Intercomparison of slant column measurements of NO<sub>2</sub> and O<sub>4</sub> by MAX-DOAS and zenith-sky UV and visible spectrometers, *Atmos. Meas. Tech.*, 3, 1629–1646, <https://doi.org/10.5194/amt-3-1629-2010>, 2010.
- Roazanov, V., Roazanov, A., Kokhanovsky, A., and Burrows, J.: Radiative transfer through terrestrial atmosphere and ocean: Software package {SCIATRAN}, *J. Quant. Spectrosc. Ra.*, 133, 13–71, <https://doi.org/10.1016/j.jqsrt.2013.07.004>, 2014.
- Sander, S., Golden, D., Kurylo, M., Moortgat, G., Wine, P., Ravishankara, A., Kolb, C., Molina, M., Finlayson-Pitts, B., and Huie, R.: *Chemical kinetics and photochemical data for use in atmospheric studies evaluation number 15*, Tech. rep., 2006.
- Schreier, S. F., Richter, A., Wittrock, F., and Burrows, J. P.: Estimates of free-tropospheric NO<sub>2</sub> and HCHO mixing ratios derived from high-altitude mountain MAX-DOAS observations at midlatitudes and in the tropics, *Atmos. Chem. Phys.*, 16, 2803–2817, <https://doi.org/10.5194/acp-16-2803-2016>, 2016.
- Simpson, R., Denison, L., Petroschevsky, A., Thalib, L., and Williams, G.: Effects of ambient particle pollution on daily mortality in Melbourne, 1991–1996, *J. Expo. Sci. Env. Epid.*, 10, 488–496, 2000.
- Simpson, R., Williams, G., Petroschevsky, A., Best, T., Morgan, G., Denison, L., Hinwood, A., Neville, G., and Neller, A.: The short term effects of air pollution on daily mortality in four Australian cities, *Aust. NZ J. Public Heal.*, 29, 205–212, 2005.
- Stemmler, K., Ammann, M., Donders, C., Kleffmann, J., and George, C.: Photosensitized reduction of nitrogen dioxide on humic acid as a source of nitrous acid, *Nature*, 440, 1476–4687, 2006.
- Stutz, J., Oh, H.-J., Whitlow, S. I., Anderson, C., Dibb, J. E., Flynn, J. H., Rappengluck, B., and Lefer, B.: Simultaneous DOAS and mist-chamber IC measurements of HONO in Houston, TX, *Atmos. Environ.*, 44, 4090–4098, 2010.
- Su, H., Cheng, Y., Oswald, R., Behrendt, T., Trebs, I., Meixner, F. X., Andreae, M. O., Cheng, P., Zhang, Y., and Pöschl, U.: Soil nitrite as a source of atmospheric HONO and OH radicals, *Science*, 333, 1616–1618, 2011.
- Thalman, R. and Volkamer, R.: Temperature dependent absorption cross-sections of O<sub>2</sub>–O<sub>2</sub> collision pairs between 340 and 630 nm and at atmospherically relevant pressure, *Phys. Chem. Chem. Phys.*, 15, 15371–15381, 2013.
- VandenBoer, T., Markovic, M., Sanders, J., Ren, X., Pusede, S., Browne, E., Cohen, R., Zhang, L., Thomas, J., and Brune, W.: Evidence for a nitrous acid (HONO) reservoir at the ground surface in Bakersfield, CA, during CalNex 2010, *J. Geophys. Res.-Atmos.*, 119, 9093–9106, 2014.
- VandenBoer, T. C., Brown, S. S., Murphy, J. G., Keene, W. C., Young, C. J., Pszenny, A., Kim, S., Warneke, C., Gouw, J. A., and Maben, J. R.: Understanding the role of the ground surface in HONO vertical structure: High resolution vertical profiles during NACHTT-11, *J. Geophys. Res.-Atmos.*, 118, <https://doi.org/10.1002/jgrd.50721>, 2013.
- VandenBoer, T. C., Young, C. J., Talukdar, R. K., Markovic, M. Z., Brown, S. S., Roberts, J. M., and Murphy, J. G.: Nocturnal loss and daytime source of nitrous acid through reactive uptake and displacement, *Nat. Geosci.*, 8, 55–60, 2015.
- Vlemmix, T., Hendrick, F., Pinardi, G., De Smedt, I., Fayt, C., Hermans, C., Piters, A., Wang, P., Levelt, P., and Van Roozendaal, M.: MAX-DOAS observations of aerosols, formaldehyde and nitrogen dioxide in the Beijing area: comparison of two profile retrieval approaches, *Atmos. Meas. Tech.*, 8, 941–963, <https://doi.org/10.5194/amt-8-941-2015>, 2015.
- Vogel, L., Sihler, H., Lampel, J., Wagner, T., and Platt, U.: Retrieval interval mapping: a tool to visualize the impact of the spectral retrieval range on differential optical absorption spectroscopy evaluations, *Atmos. Meas. Tech.*, 6, 275–299, <https://doi.org/10.5194/amt-6-275-2013>, 2013.
- Volkamer, R., Baidar, S., Campos, T. L., Coburn, S., DiGangi, J. P., Dix, B., Eloranta, E. W., Koenig, T. K., Morley, B., Ortega, I., Pierce, B. R., Reeves, M., Sinreich, R., Wang, S., Zondlo, M. A., and Romashkin, P. A.: Aircraft measurements of BrO, IO, glyoxal, NO<sub>2</sub>, H<sub>2</sub>O, O<sub>2</sub>–O<sub>2</sub> and aerosol extinction profiles in the tropics: comparison with aircraft/ship-based in situ

- and lidar measurements, *Atmos. Meas. Tech.*, 8, 2121–2148, <https://doi.org/10.5194/amt-8-2121-2015>, 2015.
- Wagner, T., Dix, B., Friedeburg, C. v., Frieß, U., Sanghavi, S., Sinreich, R., and Platt, U.: MAX-DOAS O<sub>4</sub> measurements: A new technique to derive information on atmospheric aerosols – Principles and information content, *J. Geophys. Res.-Atmos.*, 109, D22205, <https://doi.org/10.1029/2004JD004904>, 2004.
- Wagner, T., Beirle, S., Brauers, T., Deutschmann, T., Frieß, U., Hak, C., Halla, J. D., Heue, K. P., Junkermann, W., Li, X., Platt, U., and Pundt-Gruber, I.: Inversion of tropospheric profiles of aerosol extinction and HCHO and NO<sub>2</sub> mixing ratios from MAX-DOAS observations in Milano during the summer of 2003 and comparison with independent data sets, *Atmos. Meas. Tech.*, 4, 2685–2715, <https://doi.org/10.5194/amt-4-2685-2011>, 2011.
- Wagner, T., Beirle, S., Remmers, J., Shaiganfar, R., and Wang, Y.: Absolute calibration of the colour index and O<sub>4</sub> absorption derived from Multi AXis (MAX-)DOAS measurements and their application to a standardised cloud classification algorithm, *Atmos. Meas. Tech.*, 9, 4803–4823, <https://doi.org/10.5194/amt-9-4803-2016>, 2016.
- Wang, S., Cuevas, C. A., Frieß, U., and Saiz-Lopez, A.: MAX-DOAS retrieval of aerosol extinction properties in Madrid, Spain, *Atmos. Meas. Tech.*, 9, 5089–5101, <https://doi.org/10.5194/amt-9-5089-2016>, 2016.
- Wang, Y., Beirle, S., Hendrick, F., Hilboll, A., Jin, J., Kyuberis, A. A., Lampel, J., Li, A., Luo, Y., Lodi, L., Ma, J., Navarro, M., Ortega, I., Peters, E., Polyansky, O. L., Remmers, J., Richter, A., Puentedura, O., Van Roozendaal, M., Seyler, A., Tennyson, J., Volkamer, R., Xie, P., Zobov, N. F., and Wagner, T.: MAX-DOAS measurements of HONO slant column densities during the MAD-CAT campaign: inter-comparison, sensitivity studies on spectral analysis settings, and error budget, *Atmos. Meas. Tech.*, 10, 3719–3742, <https://doi.org/10.5194/amt-10-3719-2017>, 2017.
- Weber, B., Wu, D., Tamm, A., Ruckteschler, N., Rodríguez-Caballero, E., Steinkamp, J., Meusel, H., Elbert, W., Behrendt, T., and Soergel, M.: Biological soil crusts accelerate the nitrogen cycle through large NO and HONO emissions in drylands, *P. Natl. Acad. Sci. USA*, 112, 15384–15389, 2015.
- WHO: Ambient air pollution: A global assessment of exposure and burden of disease, Tech. rep., World Health Organisation, 2016.
- Wilson, S. R.: Characterisation of  $J(\text{O}^1\text{D})$  at Cape Grim 2000–2005, *Atmos. Chem. Phys.*, 15, 7337–7349, <https://doi.org/10.5194/acp-15-7337-2015>, 2015.
- Wojtal, P., Halla, J. D., and McLaren, R.: Pseudo steady states of HONO measured in the nocturnal marine boundary layer: a conceptual model for HONO formation on aqueous surfaces, *Atmos. Chem. Phys.*, 11, 3243–3261, <https://doi.org/10.5194/acp-11-3243-2011>, 2011.
- Wong, K. W., Tsai, C., Lefer, B., Haman, C., Grossberg, N., Brune, W. H., Ren, X., Luke, W., and Stutz, J.: Daytime HONO vertical gradients during SHARP 2009 in Houston, TX, *Atmos. Chem. Phys.*, 12, 635–652, <https://doi.org/10.5194/acp-12-635-2012>, 2012.
- Young, C. J., Washenfelder, R. A., Roberts, J. M., Mielke, L. H., Osthoff, H. D., Tsai, C., Pikelnaya, O., Stutz, J., Veres, P. R., and Cochran, A. K.: Vertically resolved measurements of nighttime radical reservoirs in Los Angeles and their contribution to the urban radical budget, *Environ. Sci. Technol.*, 46, 10965–10973, 2012.
- Zhou, X., Zhang, N., TerAvest, M., Tang, D., Hou, J., Bertman, S., Alaghmand, M., Shepson, P. B., Carroll, M. A., and Griffith, S.: Nitric acid photolysis on forest canopy surface as a source for tropospheric nitrous acid, *Nat. Geosci.*, 4, 1752–0908, 2011.